Circuit Simulations Combined with the Electromagnetic Field Analysis

Tsugumichi Shibata, *Member, IEEE*

Abstract—**In order to provide a means of rigorous simulation for wide-band and nonlinear microwave integrated circuits, the concept of a lumped device model is introduced into a three-dimensional, time-domain electromagnetic field analysis method. This makes it possible to perform both a circuit simulation including nonlinear lumped devices and an electromagnetic field analysis for distributed microwave components at the same time. As an example, the generation of picosecond pulses from a nonlinear transmission line circuit is simulated. Based on the results, the features and the validity of the method are discussed in comparison with conventional circuit simulations.**

I. Introduction

THE integration of electrical circuits has yielded many benefits in terms of low-cost and high-performance IC's. Especially from the viewpoint of wide-band high-speed circuit design technology, electrical circuit integration reduces circuit dimensions and enables treating a whole circuit as a lumped-element circuit up to a few GHz. Now that a circuit can be regarded as a lumped-element circuit, there are many kinds of available circuit simulators that can deal with linear and nonlinear devices. Therefore, there is a great deal of freedom that makes design easier. But, some inevitable limiting factors such as the increase of current density in the interconnects, the increase of parasitic line resistances and line capacitances that prevent circuit from high-speed operations, and difficulties in the handling and packaging of small IC chips, prevent further reductions in circuit dimensions. On the other hand, there has been rapid progress in the f_T and $f_{\max}$ of the transistor itself in recent years [1]. If we want to design wide-band integrated circuits that operate up to several tens of GHz in the near future, the problem of distributed effects must be addressed even for IC chips. (Consider that interconnects 500–600 μm in length have the electrical length of a quarter wavelength at frequency of 50 GHz and effective dielectric constant $\epsilon_{\text{eff}} = 7$.) In such a situation, a means of rigorous simulation that can treat both the nonlinear lumped devices and the distributed circuit element at the same time is strongly desired. Of course, the development of such a simulator, in which a circuit operating in narrow-band, but with large signal is analyzed, has been a subject of microwave circuit design research for some time.

In the conventional microwave circuit design, the SPICE-like time-domain simulator is widely used for the circuit simulation, in which ideal transmission lines can be treated. Also an alternative in order to include more complexed discontinuity effects of distributed circuit elements, the so called harmonic-balance technique [2], [3], is available in commercial microwave circuit simulators [4]. In any way, the characterization of distributed circuit elements and the circuit simulation have been performed separately. This feature had an advantage in the characterization of the distributed circuit elements in hybrid MIC's. In some cases, one can carry out this characterization directly by means of a network analyzer for measurements. In other cases, characterization can be carried out through electromagnetic field analysis. But this process must be completed prior to the circuit simulations, and it should be noted here that the circuit structures in IC chips are usually closely integrated and highly complicated compared with conventional hybrid MIC's. Therefore, such a work, i.e., classification, characterization and modeling of the vast and complex distributed structures that appear in IC chips is too difficult and time-consuming.

This paper aims at presenting a novel circuit simulation method that redresses the weak points of the above-mentioned simulators. For this purpose, the concept of lumped device model is introduced into a three-dimensional time-domain electromagnetic field analysis method, thus enabling circuit simulations combined with the electromagnetic field analysis. The distributed circuit elements are described by their material constants and physical structure in this simulation and both a circuit simulation and an electromagnetic field analysis are performed at the same time. This method has following features that are absent in conventional circuit simulations. First of all, it manages all kinds of distributed effects resulting from Maxwell's equations, while preserving the many features inherent in time-domain circuit simulators. Secondly, the method does not need a troublesome characterization process for complicated distributed circuit elements because this process is involved in the simulations implicitly by means of the simultaneously progressing electromagnetic field analysis. That is, the structures are analyzed

Manuscript received March 12, 1991; revised July 1, 1991.

The author is with the Integrated Circuit Technology Lab., NTT LSI Laboratories, 3-1, Morinosato Wakamiya, Atsugi-shi, Kanagawa, 243-01, Japan.

IEEE Log Number 9102823.

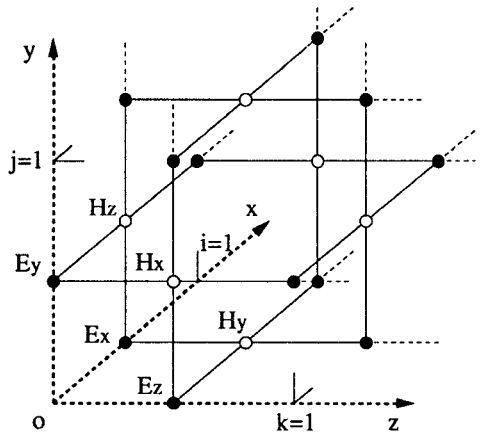

Fig. 1. Discretization of electromagnetic field variables in three-dimensional space for time-domain analysis.

only as far as necessary. Moreover, as a result of the above feature, our method, in principle, yields more rigorous results because it is free from the approximate errors occurring in the classification and characterization process of highly complicated distributed circuit elements. It also should be mentioned here that the method does require large computing power as seen quantitatively in the following chapters. We address this subject briefly in the conclusion.

II. The Method and Its Verifications

The method has as its basis a time-domain electromagnetic field analysis. Therefore, this chapter begins with a review of time-domain electromagnetic field analysis methods. After that, the formulation of a lumped device model and its numerical verifications are presented.

II-A. The Spacial Network Method (The Bergeron Method)

Today, there are three well-known methods for three-dimensional time-domain electromagnetic field analysis; the finite-difference time-domain (FDTD) method [5], the transmission line matrix (TLM) method [6] and the spacial network (SNW) method [7]. There is a close resemblance among them. Each of the above methods has a formulation for computing discretized field variables step by step in time-domain starting from an initial field distribution, accompanied by schemes for treating inhomogeneous media (dielectrics and conductors), analysis region boundaries, field excitation sources and so forth. Fig. 1 shows the discretization of field variables in three-dimensional space. In the figure, the positions of six kinds of nodes are indicated, at which the variables E_x, E_y, E_z, H_x, H_y and H_z are defined directly or correspondingly with the voltage variables of the equivalent network. The FDTD method calculates the field evolution by making a set of finite difference expression of Maxwell's curl equations directly based on the definition of Fig. 1. On the other hand, the other two make use of the equivalent network concept, the circuit equations of which are equivalent to the finite difference expression of Maxwell's equations. To solve this network, the scattering matrices at the nodes are handled in the TLM, while the nodal voltage and current equations are calculated in the SNW. Recently, these methods have been extensively applied to microwave passive device characterization, demonstrating their applicability and the validity for CAD [8]–[10]. For the purpose of this paper, any of three could be the basis of the discussions. As an example, in the following the SNW method is used.

A part of the equivalent network used in the SNW is depicted in Fig. 2. This figure shows one unit of the periodic network and corresponds to an eighth of a cell shown in Fig. 1 in volume. The equivalent network (spacial network) consists of the transmission lines, positive and negative gyrators, capacitances and conductances (these capacitances and conductances are omitted in Fig. 2, but shown in Fig. 3). The transmission lines have a characteristic impedance equal to the free space impedance $Z_0 = 377\ \Omega$ and an electrical length equal to half of the physical length $\Delta/2$. One can find that a set of circuit equations around an arbitrary node becomes formally equivalent to the set of Maxwell's partial difference equations under the condition of $\Delta \to 0$ (with the order of Δ). Therewith, the correspondence between the spacial network parameters and the field parameters can be deduced as summarized in Table I. Therefore, the analysis of the electromagnetic field is equivalent to the analysis of the spacial network. To show how to solve this spacial network in the time domain, let us turn our attention to the arbitrary Ey-node shown in Fig. 3. This nodal voltage corresponds to the Ey field component of this point. We adopt the Bergeron's method to the transmission line branches around the node. So, the following set of equations can be written with respect to the nodal voltages $V_y, V^*_{x-}, V^*_{x+}, V^*_{z-}, V^*_{z+}$ and the branch currents I_{zi}, I_{zo}, I_{xi}, I_{xo}, I^*_{zo}, I^*_{zi}, I^*_{xo}, I^*_{xi}, I_d and I_c:

$$V_y(t) + Z_0 I_{zi}(t) = I^*_{zo}(t-\Delta t) + Z_0 V^*_{x-}(t-\Delta t), \quad (1a)$$

$$V_y(t) - Z_0 I_{zo}(t) = I^*_{zi}(t-\Delta t) - Z_0 V^*_{x+}(t-\Delta t), \quad (1b)$$

$$V_y(t) + Z_0 I_{xi}(t) = I^*_{xo}(t-\Delta t) + Z_0 V^*_{z-}(t-\Delta t), \quad (1c)$$

$$V_y(t) - Z_0 I_{xo}(t) = I^*_{xi}(t-\Delta t) - Z_0 V^*_{z+}(t-\Delta t), \quad (1d)$$

$$I_d(t) = G V_y(t), \quad (1e)$$

$$V_y(t) - \frac{\Delta t}{2C} I_c(t) = V_y(t-\Delta t) + \frac{\Delta t}{2C} I_c(t-\Delta t), \quad (1f)$$

$$I_{zi}(t) - I_{zo}(t) + I_{xi}(t) - I_{xo}(t) - I_d(t) - I_c(t) = 0, \quad (1g)$$

where Δt is the electrical length of the transmission line branch in time, thus given by

$$\Delta t = \frac{\Delta}{2c}, \quad (2)$$

in which c is the wave velocity in free space. From

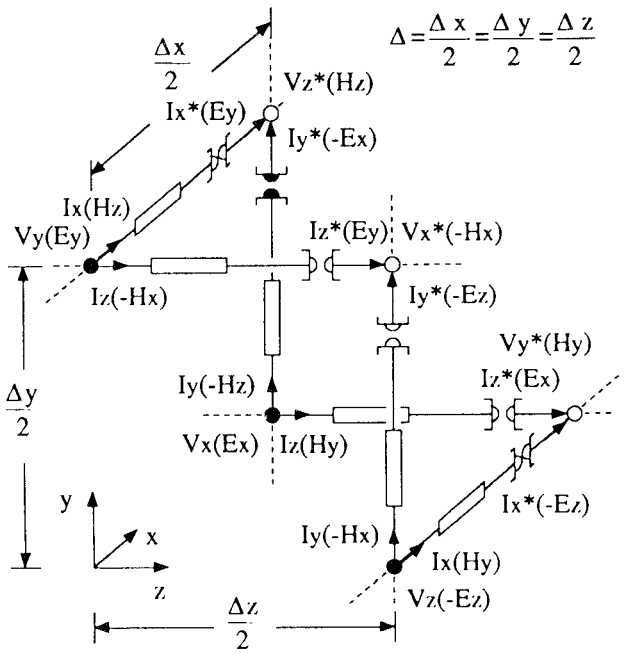

Fig. 2. Part of the spacial network.

(1a)–(1g), $V_y(t)$ can be expressed by

$$V_y(t) = \frac{R_c(\psi_1^* + \psi_2^* + \psi_3^* + \psi_4^*) + Z_0\psi_c}{Z_0 + R_c(4 + GZ_0)} \tag{3}$$

where, $R_c = \Delta t/2c$, ψ_1^*, ψ_2^*, ψ_3^*, ψ_4^* and ψ_c are the right hands of (1a)–(1d), and (1f), respectively. By using (3), $V_y(t)$ can be calculated from the values at the time $t - \Delta t$. Then the currents at the time t are also determined using (1a)–(1f) again. Similar equations can be written at every node appearing in Fig. 2. Thus, the response of the spacial network is computed step by step in time, enabling the calculation of electromagnetic field transition in the time domain.

II-B. Formulation of the Lumped Devices and Computational Examples for Verification

Simulations of distributed passive circuits using the SNW have been reported in a former paper [8], so details are not included in this paper. What we consider here is how to introduce the lumped devices into these simulations. In this section, we are concerned with the lumped resistor and the lumped capacitor, which are fundamental in device models. (The need for the lumped inductor model occurs in IC chips merely because the magnetic materials or the equivalent effects are not used in common IC chips.) On the basis of this consideration, the diode model is treated in the next chapter.

These models can be introduced in an arbitrary E-node of the spacial network by making the following assumptions:

1) An arbitrary node of the spacial network has the fictitious volume of $\Delta x \times \Delta y \times \Delta z$. In Fig. 1, one can find that each kind of node exists at the rate of one per $\Delta x \times \Delta y \times \Delta z$.

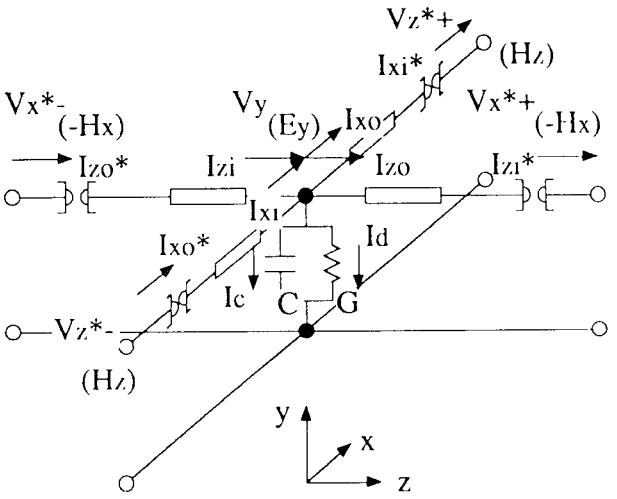

Fig. 3. Ey-node and its vicinity.

2) The lumped device is small enough to be expressed in the arbitrary node. The physical structure and the shape of the device are immaterial.

3) The device is characterized in terms of its port voltage and current, where the port voltage $V_{RF}(t)$ is given by

$$V_{RF}(t) = \int_{-\Delta}^{\Delta} \mathrm{Eds} = V_u(t) \times 2\Delta, \tag{4}$$

where $V_u(t)$; $u = x$ or y or z, is the nodal voltage of the E-node in which the device is expressed.

To explain concretely, consider a most simple circuit fabricated on GaAs substrate (dielectric constant $\epsilon_{GaAs} = 13$), i.e., the coplanar strips (CPS) terminated by a lumped resistor R_{end}. Suppose the analysis region of $0 \leqslant i \leqslant 40$, $0 \leqslant j \leqslant 80$ and $0 \leqslant k \leqslant 250$ in Fig. 1 with $2\Delta = \Delta x = \Delta y = \Delta z = 5$ μm and set the coplanar plane of the circuit to the plane $j = 40$. Fig. 4 shows a part of this plane, in which the circuit pattern is illustrated. The CPS is laid along the z-direction and a half of the structure is disposed in this analysis region under the consideration of structural symmetry, thus the plane $i = 40$ is the symmetrical plane with the electric wall condition. The Ex- and Ez-nodes appearing in the coplanar plane are indicated by closed circles, and the Hy-nodes by open circles. The CPS has the conductor width W of 20 μm and the spacing S of 30 μm. In this figure, the terminating resistor is divided into two parts by the symmetrical plane and a half, i.e., $R_{lump} = R_{end}/2$ is indicated by the hatched region, which is connected to the end of the CPS conductor through the lead conductor pattern of 10 μm. Now, consider that the Ex-node at the center of the hatched region is accompanied with the above-assumed fictitious cube. Then, the resistance between the opposite faces $\Delta y \times \Delta z$ of this cube is $(2\Delta\sigma_x)^{-1}$. Referring to the relationship in Table I, the following simple equation is derived between the lumped resistor R_{lump} and the spa-

TABLE I
CORRESPONDENCE BETWEEN THE SPACIAL NETWORK PARAMETERS AND THE ELECTROMAGNETIC FIELD PARAMETERS

	Network Parameters	Field Parameters		Network Parameters	Field Parameters
E_x-node	V_x	E_x	H_x-node	V_x^*	$-H_x$
	I_y	$-H_z$		I_y^*	$-E_z$
	I_z	H_y		I_z^*	E_y
	C	$2\epsilon_0(\epsilon_{sx}-1)\Delta$		C^*	$2\mu_0(\mu_{sx}-1)\Delta$
	G	$2\sigma_x\Delta$		G^*	$2\sigma_x^*\Delta$
E_y-node	V_y	E_y	H_y-node	V_y^*	H_y
	I_z	$-H_x$		I_z^*	E_x
	I_x	H_z		I_x^*	$-E_z$
	C	$2\epsilon_0(\epsilon_{sy}-1)\Delta$		C^*	$2\mu_0(\mu_{sy}-1)\Delta$
	G	$2\sigma_y\Delta$		G^*	$2\sigma_y^*\Delta$
E_z-node	V_z	$-E_z$	H_z-node	V_z^*	H_z
	I_x	H_y		I_x^*	E_y
	I_y	$-H_x$		I_y^*	$-E_x$
	C	$2\epsilon_0(\epsilon_{sz}-1)\Delta$		C^*	$2\mu_0(\mu_{sz}-1)\Delta$
	G	$2\sigma_z\Delta$		G^*	$2\sigma_z^*\Delta$

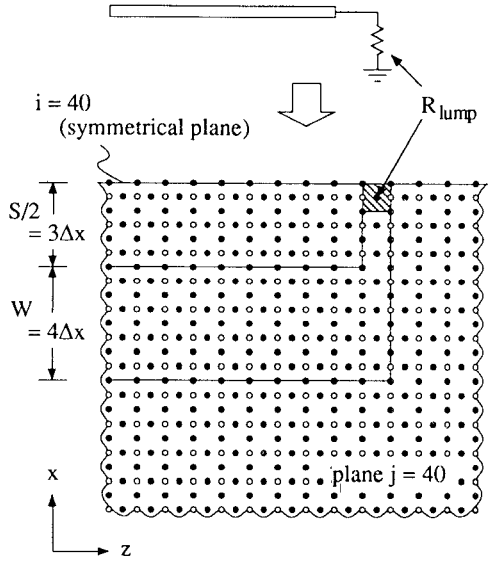

Fig. 4. Coplanar strips terminated by a lumped resistor $R_{end} = 2R_{lump}$ and a part of the coplanar plane in the spacial network.

cial network parameter G:

$$G = \frac{1}{R_{lump}}. \tag{5}$$

Thus, the Ex-node is expected to act as lumped resistor R_{lump} by setting the spacial network parameter G of this node to the value given by (5). To prove the validity of the above argument, examples were evaluated numerically. Fig. 5(a) shows the simulated standing wave amplitude along the CPS when the CPS is driven by a 50 GHz sinusoidal source at the end of $z = 0$ and terminated by the lumped resistor R_{end} at $z = 200\Delta z$. Fig. 6 presents the S-parameters of the termination calculated at the reference plane—500 μm before the termination (this was calculated by applying the FFT to the simulated pulse response of the circuit [8]). According to the conformal mapping calculation based on the quasi-static analysis of the line cross section, the characteristic impedance Z_0 of

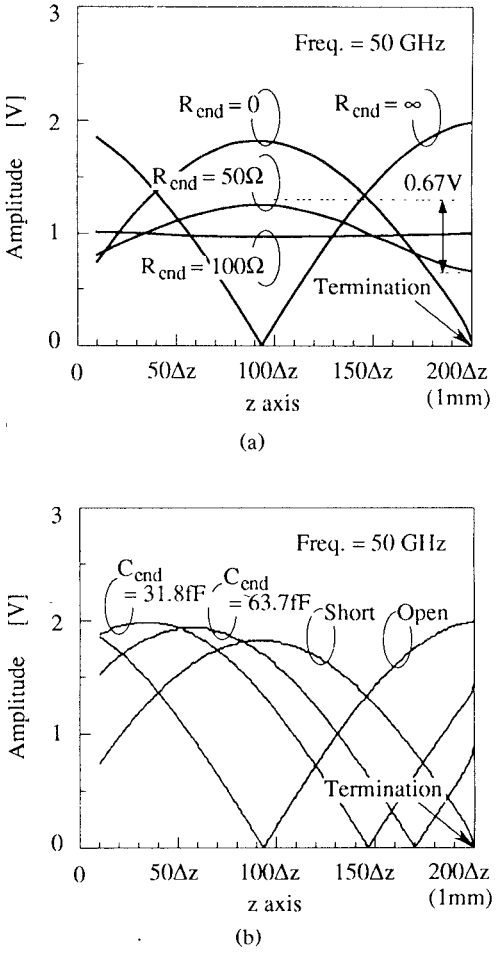

Fig. 5. Simulated standing wave distribution. (a) When the CPS is terminated by the resistor R_{end}. (b) When the CPS is terminated by the capacitor C_{end}.

the CPS is about 100 Ω. As is expected in Fig. 5(a), the reflection is hardly recognized in the case of R_{end} = 100 Ω, and the SWR of around 0.33 is obtained in the case of $R_{end} = 50$ Ω. The results in Fig. 6 likewise show good agreement with the expected values within less than ten percent error, thus demonstrating the validity of the

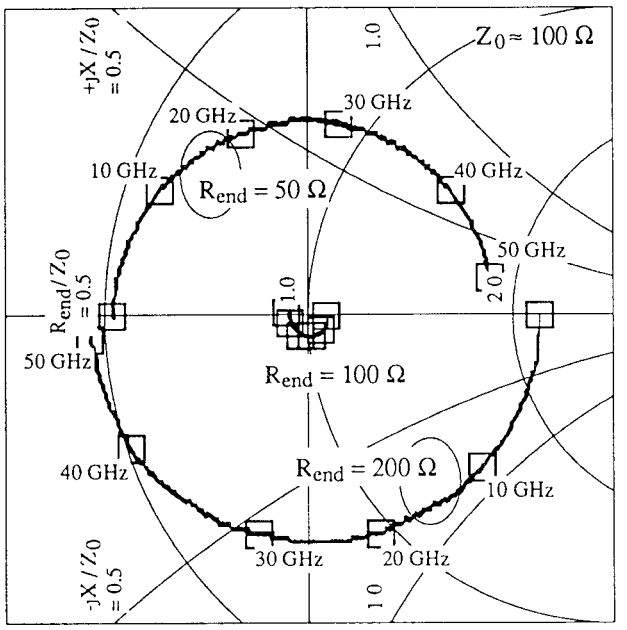

Fig. 6. The S-parameter of the termination R_{end} calculated at the reference plane of 500 μm before the termination.

assumptions and the methodology mentioned above. The small discrepancy is due to an error in the characteristic impedance Z_0 of the CPS caused by the relatively rough discretization.

A similar approach can be taken for the lumped capacitor model. Consider that the CPS is terminated by a lumped capacitor C_{end}. In this case, the hatched region in Fig. 4 represents the lumped capacitor C_{lump}, where $C_{lump} = 2C_{end}$. In order to assign this role to the Ex-node at the center of the hatched region, we should set the spacial network parameter C as

$$C = C_{lump} - 2\Delta\epsilon_0, \tag{6}$$

because the capacitance between the opposite faces $\Delta y \times \Delta z$ of the cube attendant on the Ex-node is given by $2\Delta\epsilon_0\epsilon_{sx}$. Fig. 5(b) shows results similar to Fig. 5(a) based on the above-mentioned methodology. We expected that the short point when the CPS is terminated by the capacitor $C_{end} = 3.18$ fF would be located at the middle point between the short points of the open-load case and the short-load case because we determined the value of C_{end} to satisfy $\omega C_{end} Z_0 = 1$. The result agrees with this expectation quite well, thus again demonstrating the validity of the above methodology.

III. Simulation of Nonlinear Transmission Line

In the previous chapter, we demonstrated how the lumped resistor and capacitor models can be introduced into the electromagnetic field analysis. In this chapter, we extend the model to describe the diode device and discuss the features of this simulation in terms of a simulation of picosecond pulse generation from a nonlinear transmission line circuit.

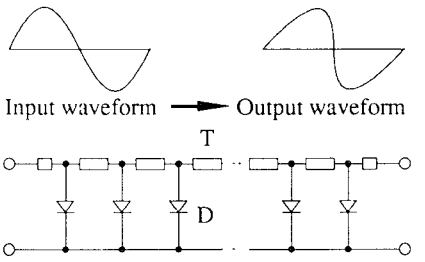

Fig. 7. Circuit diagram of the nonlinear transmission line (NLTL).

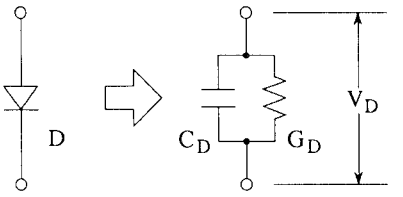

Fig. 8. Diode model used in the simulation.

III-A. Nonlinear Transmission Line for Picosecond Pulse Generation and Its Simulations Combined with the Electromagnetic Field Analysis

The nonlinear transmission line (NLTL) circuit [11] is illustrated in Fig. 7. This is a transmission line periodically loaded with Schottky varactor diodes. The signal propagation velocity of the NLTL is estimated by

$$v(V_{RF}) = \frac{1}{\sqrt{L_l(C_l + nC_D(V_{RF}))}}, \tag{7}$$

where L_l and C_l are the line inductance and the line capacitance per unit length without the loaded diodes, n is the number of the loaded diodes per unit length, and $C_D(V_{RF})$ is the capacitance of the diode as a function of its port voltage V_{RF}. The voltage-dependent characteristics of the propagation velocity provide some applications such as the voltage-controlled phase-shifters and the picosecond pulse generators. If the NLTL is driven by a large-signal sinusoidal source, a negative-going transition is sharpened as the wave propagates because the negative half cycle of the waveform propagates faster than the positive half cycle. Generated picosecond electrical transition is attractive in the area of high-speed signal processing and is used, for example, for gating the sampling switch [12]. The following gives the simulation of the picosecond pulse generation combined with the electromagnetic field analysis.

In the simulation, we represented the diode by a parallel connection of a nonlinear capacitance C_D and a nonlinear conductance G_D, as shown in Fig. 8. Their values depend on the port voltage $V_{RF} \equiv V_D$ as follows:

$$C_D = \frac{C_{j0}}{\sqrt{1 - V_D / V_B}} \tag{8}$$

$$G_D = \frac{I_D}{V_D}; \qquad I_D = I_S(e^{V_D/NV_T} - 1) \tag{9}$$

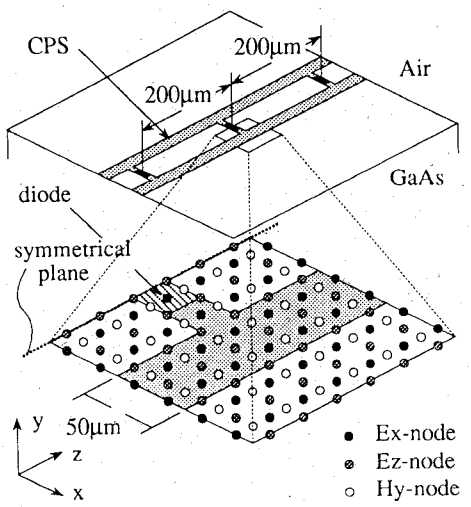

Fig. 9. Monolithic GaAs NLTL and its analysis condition.

where, $C_{j0} = 62.6$ fF, $V_B = 0.65$ V, $I_S = 18.4$ pA, $N = 1.5$ and $V_T = 25.85$ mV. The values of the spacial network parameters G and C at the nodes of the diode models were varied at every time step to satisfy (8) and (9) together with the relation of (5) and (6) as a function of V_D evaluated by (4). The simulated NLTL is a monolithic GaAs NLTL. The CPS on the GaAs substrate ($W = 50$ μm, $S = 100$ μm) is periodically loaded with the diodes at spacings of 200 μm. Fig. 9 shows the circuit structure and an enlarged pattern around the diode. The spacial network of a size equal to $20\Delta x \times 40\Delta y \times 1000\Delta z$ where $2\Delta = \Delta x = \Delta y = \Delta z = 25$ μm is used for the analysis, in which the line is laid along the z-direction and the plane $x = 0$ is the symmetrical plane with the electric wall condition under the consideration of structural symmetry. The plane $y = 20\Delta y$ is the coplanar plane of the circuit. Every Ex-node at the center of the hatched region indicated in Fig. 9 represents the diode model. Fig. 10(a) shows the simulated waveforms when the NLTL is driven by a 10 GHz sinusoidal source at the end of $z = 0$. It is clearly shown that the negative-going transition of the waveform is sharpened as the propagating distance increases and that the fall time can be compressed to the picosecond domain.

III-B. Discussions

Fig. 10(b) shows the result of conventional simulation and it is comparable with the result of Fig. 10(a). The result in Fig. 10(b) was obtained by solving the circuit shown in Fig. 7 using the Bergeron's method as a numerical instrumentality, i.e., the transmission line T was treated as an idealized one that has a constant characteristic impedance $Z_0 = 111$ Ω, a fixed electrical length Δt (determined from the effective dielectric constant $\epsilon_{\text{eff}} = 7$ and the spacing of 200 μm) and no loss. Such a result can also be obtained by utilizing a common time-domain circuit simulator. One important difference found between the results in Fig. 10(a) and (b) is in the cycle of the characteristic oscillation that appears after the sharpened

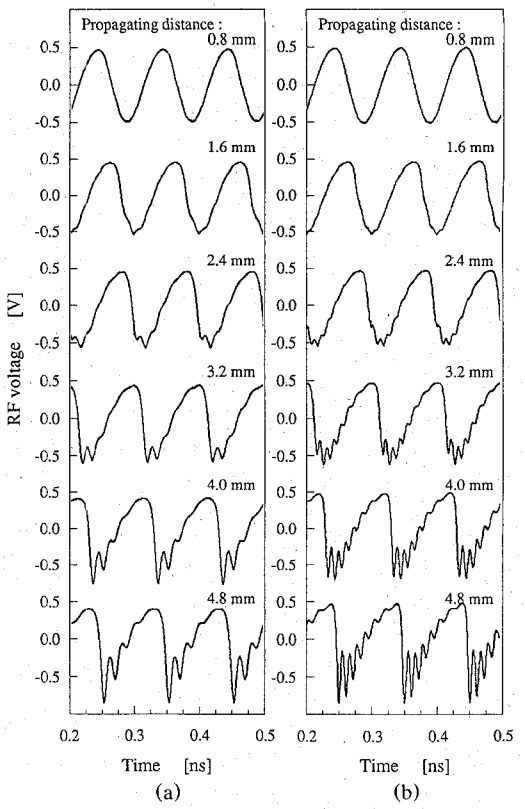

Fig. 10. Simulated waveforms of the NLTL. (a) Result of the proposed simulation. (b) Result of the conventional simulation.

edge of the waveform. Fig. 10(a) shows longer cycle than that in (b). This characteristic oscillation is caused by the Bragg reflection owing to the periodic structure of the NLTL and limits the final compressible fall time. Namely, the NLTL has a cutoff frequency roughly estimated by

$$\omega_{\text{per}} \approx \frac{2n}{\sqrt{L_l(C_l + nC_D)}} \tag{10}$$

and no harmonics at frequencies higher than ω_{per} can be generated. The above-mentioned difference should be brought about by the following reasons:

1) The result in (a) takes into account the effect of the parasitic capacitances and inductances attendant on the lead conductors connecting the diode port and the CPS line, while it is neglected in result (b). This effect leads to decreased ω_{per} making the cycle of the characteristic oscillation longer. 2) The frequency dispersion effect inherent in the CPS line is included in result (a).

The effective dielectric constant of the monolithic GaAs CPS is constant up to several tens of GHz but increases with frequency in the higher frequency region [10]. Although this effect may be perturbed by the loaded diodes, an influence that decreases ω_{per} is thought to exist. Such an effect is rigorously simulated in result (a). To conclude the discussions, the proposed circuit simulation can provide rigorous results that include various distributed and structural effects. These effects, which can hardly be handled by conventional simulators, are gaining great importance in high-speed IC design technology.

IV. Conclusion

A rigorous simulation method for the wide-band and nonlinear high-speed IC's has been presented in this paper. By introducing the concept of lumped device model into the three-dimensional time-domain electromagnetic field analysis method, circuit equations, i.e., the voltage-current equations of the lumped devices, as well as the electromagnetic field distributions are solved simultaneously in the time domain. Using examples of circuits, we have demonstrated how to treat the resistor model, the capacitor model and the diode model. The simulations of the examples yield satisfactory results, showing the validity and the necessity of these simulations.

To further extend the variety of the models, dependent sources, such as the transconductance, will be introduced by using a set of two nodes of the spacial network, in which the field excitation source connects with the one node assigned to the output port and the other node is used as the input port to control the source.

Currently, the need for large computing power limits the practical use of this method. The example simulations need to handle about 4 800 000 nodes and 10–12 words/node of the memory must be addressed. Therefore, the use of a supercomputer is indispensable. It is expected that progress in computing power and supercomputer popularization will make the method more feasible in the practical design of future IC's.

Acknowledgment

The motivation for this work was brought up in an informal meeting with Associate Professor N. Yoshida of Hokkaido University a few years ago and a preliminary study was done by H. Kimura, a graduate student of Hokkaido University, when he visited our laboratory in August 1990. The author would like to thank them for their contributions. Also the discussions and the encouragements of Dr. A. Iwata, Y. Akazawa and Dr. N. Ieda, NTT LSI Laboratories, are greatly appreciated.

References

[1] P. C. Phao, A. J. Tessmer, K.-H. G. Duh, P. Ho, M.-Y. Kao, P. M. Smith, J. M. Ballingall, S.-M. J. Liu, and A. A. Jabra, "W-Band low-noise InAlAs/InGaAs lattice-matched HEMT's," *IEEE Electron Device Lett.*, vol. EDL-11, pp. 59–62, Jan. 1990.

[2] V. Rizzoli and A. Neri, "State of the art and present trends in nonlinear microwave CAD techniques," *IEEE Trans. Microwave Theory Tech.*, vol. MTT-36, pp. 343–365, Feb. 1988.

[3] K. S. Kundert, G. B. Sorkin, and A. S. Vincentelli, "Applying harmonic balance to almost-periodic circuits," *IEEE Trans. Microwave Theory Tech.*, vol. MTT-36, pp. 366–378, Feb. 1988.

[4] Libra: EESof Inc., Microwave Harmonica: Compact Software Inc., and HP Microwave Design System, Hewlett-Packard Co..

[5] K. S. Yee, "Numerical solution of initial boundary value problems involving Maxwell's equations in isotropic media," *IEEE Trans. Antennas Propagat.*, vol. AP-14, pp. 302–307, May 1966.

[6] P. B. Johns, "The solution of inhomogeneous waveguide problems using a transmission-line matrix," *IEEE Trans. Microwave Theory Tech.*, vol. MTT-22, pp. 209–215, Mar. 1974.

[7] N. Yoshida, I. Fukai, and J. Fukuoka, "Transient analysis of three-dimensional electromagnetic fields by nodal equations," *Trans. IECE Japan*, vol. 63-B, pp. 876–883, Sept. 1980.

[8] T. Shibata, T. Hayashi, and T. Kimura, "Analysis of microstrip circuits using three-dimensional full-wave electromagnetic field analysis in the time domain," *IEEE Trans. Microwave Theory Tech.*, vol. MTT-36, pp. 1064–1070, June 1988.

[9] T. Shibata and E. Sano, "Analysis of coplanar lines utilizing the time-domain finite difference technique," *Trans. IEICE Japan*, vol. J73-C-I, pp. 61–70, Feb. 1990.

[10] ____, "Characterization of MIS structure coplanar transmission lines for investigation of signal propagation in integrated circuit," *IEEE Trans. Microwave Theory Tech.*, vol. MTT-38, pp. 881–890, July 1990.

[11] C. J. Madden, M. J. W. Rodwell, R. A. Marsland, D. M. Bloom, and Y. C. Pao, "Generation of 3.5 ps fall-time shock waves on a monolithic GaAs nonlinear transmission line," *IEEE Electron Device Lett.*, vol. EDL-9, pp. 303–305, Jun. 1988.

[12] R. Y. Yu, M. Case, M. Kamegawa, M. Sundaram, M. J. W. Rodwell, and A. W. Gossard, "275 GHz 3-Mask Integrated GaAs Sampling Circuit," *Electronics Letters*, vol. 26, pp. 949–951, June 1990.

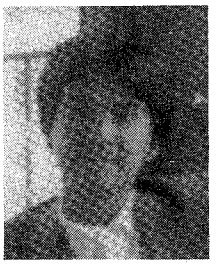

Tsugumichi Shibata (M'87) was born in Tokyo, Japan, on July 14, 1959. He received the B.S. and M.S. degrees in electrical engineering from the University of Tokyo, Tokyo, Japan, in 1983 and 1985, respectively.

In 1985, he joined the Atsugi Electrical Communications Laboratories, Nippon Telegraph and Telephone Corporation, Atsugi, Japan. He has been engaged in research on electromagnetic field analysis, electro-optic sampling of subpicosecond signal in IC chips, and the design of high-speed devices and circuits for data acquisition system. His interests also include the analysis of quantum effect devices and the design of OEICs.

Mr. Shibata is a member of the Institute of Electronics, Information and Communication Engineers of Japan and the Japan Society of Applied Physics.